Revah, F., Galzi, J.-L., Giraudat, J., Haumont, P.-Y., Lederer, F., & Changeux, J.-P. (1990) *Proc. Natl. Acad. Sci. U.S.A. 87*, 4675–4679.
Schaffner, W., & Weissmann, C. (1973) *Anal. Biochem. 56*, 502–514.
Singh, S. P., Stenberg, V. I., & Parmar, S. S. (1980) *Chem. Rev. 80*, 269–282.
Sobel, A., Weber, M., & Changeux, J.-P. (1977) *Eur. J. Biochem. 80*, 215–224.
Stroud, R. M., McCarthy, M. P., & Shuster, M. (1990) *Biochemistry 29*, 11009–11023.
Toyoshima, C., & Unwin, N., (1988) *Nature (London) 336*, 247–250.
Weiland, G., & Taylor, P. (1979) *Mol. Pharmacol. 15*, 197–212.
White, B. H., & Cohen, J. B. (1988) *Biochemistry 27*, 8741–8751.
Whitten, D. G. (1976) in *Photochemistry of Heterocyclic Compounds* (Buchardt, O., Ed.) pp 524–573, John Wiley & Sons, New York.

Transbilayer Distribution of Bromine in Fluid Bilayers Containing a Specifically Brominated Analogue of Dioleoylphosphatidylcholine†

Michael C. Wiener and Stephen H. White*
Department of Physiology and Biophysics, University of California, Irvine, California 92717
Received January 22, 1991; Revised Manuscript Received April 17, 1991

ABSTRACT: We describe in this paper the transbilayer distribution of the bromines of the specifically halogenated phospholipid 1-oleoyl-2-(9,10-dibromostearoyl)-*sn*-glycero-3-phosphocholine (OBPC). The distribution was determined by X-ray diffraction of oriented multilayers of mixtures of OBPC and 1,2-dioleoyl-*sn*-glycero-3-phosphocholine (DOPC) at 66% relative humidity by the general approach of Franks et al. (1978) [*Nature 276*, 530–532]. The bromine distribution of OBPC in the fluid L_α phase is described accurately by a pair of Gaussian functions located 7.97 ± 0.27 Å from the center of the bilayer with $1/e$ half-widths of 4.96 ± 0.62 Å. We find that OBPC bilayers are accurately described as DOPC bilayers with an additional bromine distribution centered at the position of the double bond of DOPC and conclude that OBPC is an excellent structural isomorph for DOPC under the conditions of these experiments. The distribution obtained is the complete and fully resolved transbilayer image of the halogen label because the broad distribution of the bromines is due entirely to thermal disorder and not to experimental limitations [Wiener, M. C., & White, S. H. (1991a) *Biophys. J. 59*, 162–173]. The observed width of the bromine distribution indicates that virtually all of the hydrocarbon interior is accessible to the bromines. The distance between the bromine/double-bond position and the headgroup phosphate position was determined from one-dimensional Patterson maps and found to be ≈12 Å. The application of accurately determined bromine distributions to the quantitative interpretation of fluorescence quenching experiments is discussed. A method for the self-consistent global analysis of diffraction data from mixtures that permits the use of data sets with different instrumental scale factors is developed in an Appendix.

Fluorescence spectroscopy is an important experimental method for investigating biomolecules in membrane environments [see Lakowicz (1983)]. Of particular interest are fluorescence energy transfer (Kleinfeld, 1985; Kleinfeld & Lukacovic, 1985) and fluorescence quenching (Markello et al., 1985; Blatt & Sawyer, 1985; Everett et al., 1986; Chattopadhyay & London, 1987) methods used to determine the positions of fluorophores in membranes. The fluorophores are typically endogenous tryptophans of membrane proteins, labels attached to proteins, or labeled lipids. The elegant and promising "parallax method" of Chattopadhyay and London (1987) can be used to determine the depth of a fluorophore in a membrane by measuring the degree of quenching by two labels at different positions within the bilayer. However, this method, like all others, requires prior estimates of the average positions of the fluorescence quenchers (or acceptors) in order to obtain the accurate position of the donor fluorophore. In addition, the transbilayer distributions of acceptors or quenchers across the bilayer may influence the interpretation of fluorescence experiments or the theoretical models on which their interpretation is based.

Brominated lipids have been used as fluorescence quenchers (Leto et al., 1980; East & Lee, 1982; Holloway et al., 1982; Markello et al., 1985; Everett et al., 1986) and several recent papers attest to continued interest in using specifically brominated phospholipids for examining membrane structure (Silvius, 1990; Yeager & Feigenson, 1990; De Kroon et al., 1990). X-ray diffraction is an excellent method for determining the positions and distributions of heavy atoms and other labels within bilayers (Lesslauer et al., 1971, 1972; McIntosh et al., 1976; Franks et al., 1978; Lytz et al., 1984; McIntosh & Holloway, 1987; Trumbore et al., 1988; Mason et al., 1989; Katsaras & Stinson, 1990) and thus can provide crucial information for the analysis of quenching data. We describe in this paper the fully resolved transbilayer distribution of bromines of the specifically halogenated phospholipid 1-oleoyl-2-(9,10-dibromostearoyl)-*sn*-glycero-3-phosphocholine (OBPC,[1] shown in Figure 1). We have determined the

†This work was supported by grants from the National Science Foundation (DMB-880743) and the National Institute of General Medical Sciences (GM-37291).
* Author to whom correspondence should be addressed.

[1] Abbreviations: OBPC, 1-oleoyl-2-(9,10-dibromostearoyl)-*sn*-glycero-3-phosphocholine; DOPC, 1,2-dioleoyl-*sn*-glycero-3-phosphocholine; 18:1 lysoPC, 1-oleoyl-*sn*-glycero-3-phosphocholine; TLC, thin-layer chromatography; HPLC, high-performance liquid chromatography; EtOH, ethanol; MeOH, methanol.

0006-2960/91/0430-6997$02.50/0

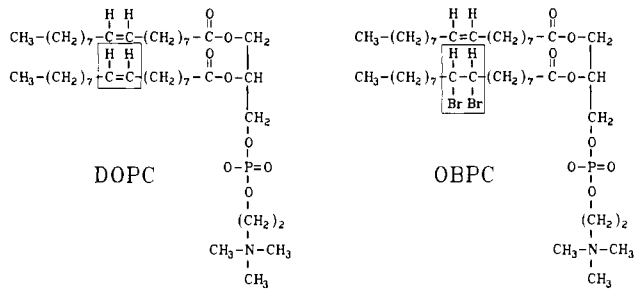

FIGURE 1: Schematic depiction of the structures of DOPC and OBPC. The oleoyl chain at the 2-position of DOPC is replaced by the 9,10-dibromostearoyl chain.

bromine distribution by an analysis of X-ray data from oriented multilayers at 66% relative humidity prepared from a series of mixtures of OBPC and 1,2-dioleoyl-*sn*-glycero-3-phosphocholine (DOPC) containing 0.00–1.00 mole fraction OBPC. The distribution of bromine atoms across the bilayer is described accurately by a pair of Gaussian functions located symmetrically 7.97 ± 0.27 Å from the center of the bilayer with $1/e$ half-widths of 4.96 ± 0.62 Å. The position of the center of scattering of the bromine label is similar to the position of the 9,10 double bond of DOPC (Jacobs & White, 1989; Wiener et al., 1991), and we conclude that OBPC is an excellent structural isomorph for DOPC under the conditions of these experiments.

Our initial interest in specifically halogenated phospholipids arose in a context removed from fluorescence applications. We are engaged in a detailed and rigorous investigation of the use of membrane diffraction methods for the determination of liquid-crystalline bilayer structure and are developing what we refer to as methods of "liquid-crystallography" (Wiener & White, 1991a,b). A fundamental aspect of these methods is the realization that typical arrays of liquid-crystalline bilayers are well represented, at least at moderate hydrations, as the convolution of a nearly perfect one-dimensional lattice with a highly thermally disordered unit cell (Wiener & White, 1991a). This situation is qualitatively different from the more familiar case of a crystal. The unit cell of a crystal with a small degree of thermal disorder is intrinsically a *high-resolution* structure so that many orders of diffraction are observed and atoms or small clusters of atoms can be resolved. In contrast, the unit cell of a liquid-crystalline bilayer has a high degree of thermal disorder so only 5–10 orders of lamellar diffraction are observed and individual atoms or small clusters of atoms are smeared together into larger "quasimolecular" distributions. These broad distributions comprise the intrinsically *low-resolution* structure of the bilayer and have characteristic widths on the order of d/h_{max} where d is the lamellar repeat and h_{max} is the highest observable diffraction order (Wiener & White, 1991a). Just as a complete set of structure factors from a crystal is sufficient to describe the fully resolved image of its intrinsically high-resolution structure, a complete set of X-ray and neutron structure factors from a liquid-crystalline bilayer is sufficient to describe fully its intrinsically low-resolution structure (Wiener & White, 1991b). The images of both crystals and thermally disordered liquid-crystals are *fully resolved* and accurate depictions of average structures determined over the time scale of the diffraction experiment.

Fully resolved images of the entire bilayer can be obtained by the use of appropriate structural models that divide the bilayer into a series of quasimolecular fragments described by Gaussian distributions (King & White, 1986; Wiener & White, 1991b). We will describe elsewhere the fully resolved structure of DOPC at 66% RH obtained by the joint refinement of neutron and X-ray diffraction data. A crucial aspect of the joint refinement procedure is the determination of the absolute values of the neutron and X-ray structure factors. The scaling of neutron diffraction data to obtain absolute values can be performed from the same experiments used to phase the structure factors. Neutron diffraction structure factors are routinely phased by carrying out experiments on samples hydrated at different D_2O/H_2O ratios (Worcester & Franks, 1976; Büldt et al., 1979; Franks & Lieb, 1979; Jacobs & White, 1989). By independently determining the water content of the unit cell, these contrast variation experiments also serve to place the neutron data on an absolute scale (Blasie et al., 1975; King et al., 1985; Jacobs & White, 1989). The structure factors at different D_2O/H_2O ratios also determine the distribution of water across the bilayer (Zaccai et al., 1975; Worcester & Franks, 1976; Franks & Lieb, 1979; Jacobs & White, 1989). Unfortunately, deuteration is not suitable for X-ray contrast variation, so another approach is required to scale the X-ray data. Franks et al. (1978) used specifically halogenated cholesterol to place X-ray scale factors on an absolute scale and demonstrated that halogenated membrane components could be satisfactory structural isomorphs in membrane diffraction. We were thus inspired to attempt to scale our X-ray data in a similar fashion. Just as neutron diffraction yields distributions of water or other specifically deuterated membrane components, the experiments of Franks et al. (1978) yielded the transbilayer distribution of the halogenated portion of cholesterol. In our study, observing all of the X-ray diffraction orders from a series of OBPC/DOPC mixtures enabled us to obtain a fully resolved image of the bromine label.

Material and Methods

Lipid Synthesis and Purification

Synthesis of OBPC. 9,10-Dibromostearic acid with a quoted purity of 99+% was obtained from Nu Chek Prep Inc., Elysian, MN. Elemental analysis (Robertson Laboratory, Inc., Madison, NJ) indicated 1.972 ± 0.013 bromines per 18 carbons for an estimate of at least 97% purity with the remainder of the material oleic acid, water, and possibly a monobrominated species. Mass spectroscopy revealed no fragments with more than two bromines. 1-Oleoyl-*sn*-glycero-3-phosphocholine (18:1 lysoPC) was obtained from Avanti Polar Lipids (Birmingham, AL), and its purity was checked by analytical thin-layer chromatography (TLC). Fatty acid anhydride was prepared by the method of Selinger and Lapidot (1966). Synthesis of OBPC from the dibromostearic acid anhydride and 18:1 lysoPC proceeded according to the protocol of Gupta et al. (1977) as modified by Runquist and Helmkamp (1988). Following isolation of the product by preparative TLC, analytical TLC of the purified OBPC revealed a single spot that migrated at approximately the same rate as DOPC. Phosphorus assays were performed by the method of Bartlett (1959), and the lipid was stored in 1:1 $CHCl_3$/MeOH (v/v) at −70 °C. The yield, estimated by the phosphorus assay, was approximately 25%.

HPLC of OBPC. We carried out reverse-phase HPLC analysis of fatty acid phenacyl esters (Longmuir et al., 1987) to quantify the amount of bromine per lipid molecule. HPLC was performed with a Rainin system consisting of two HPX pumps, a pressure monitor, a Rheodyne 7161 injection loop, and a Dynamax high-pressure mixer controlled by an Apple McIntosh SE computer running the Rainin Dynamax Method Manager. A Rainin Microsorb 5 μm C18, 25-cm bed, ana-

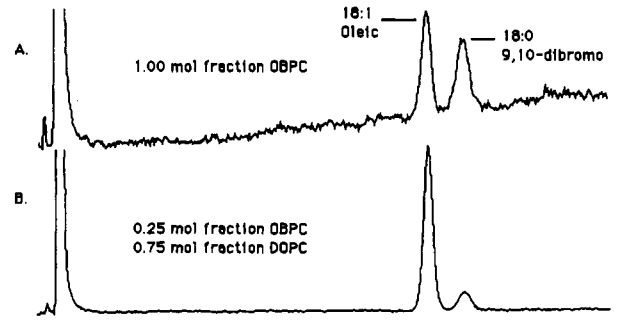

FIGURE 2: Representative HPLC chromatograms of phenacyl esters prepared from OBPC/DOPC mixtures. Approximately 10–100 nmol of a lipid mixture in 1–10 μL of acetone was injected, and 70% acetonitrile/30% H_2O (v/v) was run isocratically for 90 min at a flow rate of 1 mL/min. From the left, the first small feature is residual free phenacyl bromide in the reaction mixture that was not esterified to the fatty acid chains. Next, the large off-scale peak is the acetone carrier from the injection. The third peak is the oleic acid phenacyl ester which came off of the column with a retention time of ≈60 min. The dibromostearic acid phenacyl ester came off of the column ≈5.5 min later and is resolvable from the oleic ester peak. Phenacyl esters prepared from oleic and dibromostearic fatty acids had retention times identical with the corresponding esters prepared from hydrolyzed OBPC. The areas of the peaks were obtained by numerical integration with the interactive software provided with the HPLC system. The ratios of integrated areas are consistent with the expectation that the synthesized lipid OBPC is of high purity. (A) 1.00 mole fraction OBPC. (B) 0.25 mole fraction OBPC/0.75 mole fraction DOPC.

lytical column was used with a C4 guard column at a flow rate of 1 mL/min. Absorbance was monitored at 254 nm with a Hitachi Model 100-40 spectrophotometer equipped with high-pressure flow cell (Altex), and the photomultiplier current was recorded directly by the computer. Approximately 10–100 nmol of phenacyl ester in 1–10 μL of acetone was injected, and 70% acetonitrile/30% H_2O (v/v) was run isocratically for 60–90 min.

HPLC of carboxylic acid phenacyl esters yielded quantitative and accurate amounts of dibromostearic and oleic phenacyl esters in samples prepared from OBPC, OBPC/DOPC mixtures, and their fatty acid precursors. Figure 2 shows representative HPLC chromatograms of several OBPC/DOPC mixtures. The oleic and dibromostearic esters are clearly resolved with a peak-to-peak separation of 5.5 min; the oleic ester came off of the column first with a retention time of about 60 min. The expected values of the ratio R = dibromostearic/(oleic + dibromostearic) are 0.500 and 0.125 for 1.00 mole fraction OBPC and 0.25 mole fraction OBPC/0.75 mole fraction DOPC, respectively. Within experimental error, the calculated ratios obtained from the integrated areas of the chromatogram peaks in Figure 2 are consistent with these expectations and are not sufficient to disprove the null hypothesis, i.e., we conclude that each OBPC molecule contains one oleic and one dibromostearic acyl chain. The estimated uncertainty of the calculated ratios, estimated to be 5–10%, arises from variation in positioning of the baselines for integration. These results in conjunction with the results from elemental analysis of the bromostearic acid and other checks during the synthesis of OBPC gave us confidence that we had a pure specifically halogenated lipid with two bromines per molecule.

X-ray Diffraction

Sample Preparation and Data Collection. Oriented samples were produced with a technique adapted from Franks and Lieb (1979) and Jacobs and White (1989). Separate aliquots of OBPC and DOPC each in 1:1 $CHCl_3$/MeOH (v/v) with a combined mass of ≈1 mg were combined and vortexed vigorously for 15–30 s. Some of the solvent was gently removed with a stream of nitrogen gas to reach a final concentration of ≈1 mg of lipid/200 μL of solvent. A 2-cm length of 5-mm diameter thin-wall glass NMR tube was mounted on the shaft of a rotary vacuum evaporator motor. The lipid solution was applied dropwise to the outer surface of the rotating tube so that a uniform layer of sample was deposited upon its circumference. After the solvent evaporated, the sample was spread by applying several drops of 1:1 $CHCl_3$/MeOH (v/v) to the rotating tube and "smoothing" the lipid film with the tip of a Pasteur pipette. Samples were equilibrated in the dark for at least 24 h under argon in a sealed chamber at 66% RH, which was maintained by a reservoir containing a saturated aqueous solution of $NaNO_2$ (O'Brien, 1948). The sample was then placed inside the X-ray camera, which contained several containers of saturated $NaNO_2$ solutions. The camera was flushed with helium gas, sealed, and equilibrated for 12–24 h. The sample was positioned so that the incident X-rays were tangent to the curved surface of the oriented multilayers at a glancing angle such that all of the lamellar diffraction orders were recorded in a single experiment (Franks & Lieb, 1979). X-ray diffraction experiments were conducted with nickel-filtered Cu-K_α radiation (1.542 Å) with a modified Spectro Equipment, Inc. (North Royalton, OH) microfocus fixed-anode X-ray generator that operated at 250 W and utilized toroidal optics (Elliott, 1965). In this sample geometry, much of the wide-angle diffraction pattern was absorbed by the glass substrate and sample holder before reaching the film stack. Additional unoriented samples were prepared inside 1-mm glass capillary tubes, and more complete wide-angles patterns were recorded. All experiments were conducted at room temperature (23 °C). Because it is critical to record all of the observable diffraction orders, we conducted experiments on DOPC samples for exposure times of up to 120 h. For DOPC samples over a wide range (24–120 h) of exposure times, no systematic differences in the line widths or integrated intensities of diffraction orders were observed; we conclude that sample degradation over the course of the experiments was minimal. For all exposure times, no more than eight diffraction orders were observed, so $h_{max} = 8$. In subsequent experiments on oriented samples prepared from OBPC/DOPC mixtures, exposure times of 72 h were sufficient to record seven or eight orders of lamellar diffraction data. The wide-angle patterns from unoriented samples were recorded at shorter exposure times (4–8 h). Patterns were recorded on stacks of Kodak DEF-5 X-ray films and developed with Kodak GBX developer and fixer. After being washed in distilled water, films were dipped in dilute Kodak Photo-Flo solution and then air dried.

Film Measurement and Integration. Films were scanned with a modified Zeineh SLR-2D/1D laser densitometer (Biomed Instruments, Inc., Fullerton, CA). Our modifications include software that runs the scanner and an optical aperture that enables virtually all of the diffraction pattern from an oriented sample to be recorded in a one-dimensional film scan. Densitometer scans were processed with the GraEd software package developed by C. P. Yang (personal communication). The optical density due to background fog, which is given by the measured optical density of each film at the position of the beam-stop, was subtracted from each densitometer trace, and the films were scaled to each other by the appropriate power of the film factor f, i.e., the nth film is scaled by f^{n-1}. A film factor value of 3.2, determined by Phillips and Phillips (1985), yielded satisfactory overlap of the optical densities of the films in the stack. The uncorrected integrated intensities

$I(h)$ were obtained by two different methods: numerical integration of the area under a diffraction peak or fitting a Gaussian line shape to the diffraction peak and integrating analytically. Scattering from the glass substrate introduced nonzero backgrounds for the higher ($h \geq 6$) orders. For these higher orders, baselines used for integration were approximated by linear or quadratic functions fit to the intensities on either side of each diffraction peak, or densitometer traces of exposures recorded from the glass substrate alone were subtracted from the film scans. The values of the observed structure factors $f(h)$ were obtained from

$$|f(h)| = [h \cdot I(h) \cdot A^{-1}(h)]^{1/2}$$

where h is the Lorentz factor and $A(h)$ the absorption factor (described below). Except for pure DOPC, the structure factors for each OBPC/DOPC mixture are based upon one X-ray diffraction experiment conducted with a single sample. The DOPC data were obtained from four experiments recorded from three different samples each prepared from a different batch of DOPC. Typically, the more intense lower orders were recorded on 2–5 films in the stack during an experiment. Because the films in a stack were appropriately scaled, the integrated intensities determined from each film for a given order could be combined to determine an average intensity with associated standard deviation. Also, the integration method and the choice of baseline (for the higher orders) introduced some additional variation in the values of the integrated intensities. Each structure factor for nonzero OBPC concentrations used in this study is thus based upon 2–8 separate determinations of integrated intensity, and each structure factor for pure DOPC is based upon about four times as many determinations. The weak higher orders ($h = 6$–8) are based upon the fewest determinations as they were usually observed on only one film.

Absorption Correction. The path length that the X-rays traverse through the lipid deposited on the glass tube is longest for the low orders so that more of the incident X-rays are absorbed relative to the higher orders. While the absorption correction factor $A^{-1}(h)$ for this particular geometry has been used previously by Franks and Lieb (1979), its explicit functional form has, to our knowledge, not appeared in the literature. For a tube (or curved substrate) of radius r with a deposited sample of thickness t, the absorption $A(h)$ is given by

$$A(h) = \exp(2\mu r \sin\Theta) \int_0^t \exp\{-2\mu[(r+\xi)^2 - (r\cos\Theta)^2]^{1/2}\}\, d\xi \quad (1)$$

The angle Θ is determined by Bragg's law, $2d \sin\Theta = h\lambda$, and μ is the linear absorption coefficient of the lipid calculated from the mass absorption coefficients of its constituent atoms by the method of Johns and Cunningham (1983). The value of μ ranged from 8.0 cm^{-1} for DOPC to 20.4 cm^{-1} for OBPC. The largest corrections are for the first orders; for the estimated film thickness of 10 ± 5 μm and the bilayer repeat d of 49.1 Å, A^{-1} ($h = 1$) ranged from 1.13 ± 0.04 for DOPC to 1.36 ± 0.12 for OBPC. As a consistency check, the corrected intensities $|f(h)|^2$ obtained from oriented samples of DOPC were compared to the intensities $|f'(h)|^2 = h^2 I'(h)$ obtained from unoriented dispersions of DOPC and found to be in good agreement.

Scaling. Ideally, one wishes to obtain a bilayer density profile from X-ray diffraction that is on the absolute scale where the distribution of matter in the bilayer is described on a per volume basis, i.e., scattering length or electrons per cubic ångström. However, lamellar diffraction experiments provide information solely on the one-dimensional density projection along the bilayer normal, and determination of the absolute (per volume) scale requires knowledge of the average lipid area S, which is not determined from the diffraction experiment. White and co-workers (King et al., 1985; White & Jacobs, 1989; Wiener & White, 1991b) developed a convenient "relative absolute" scale that permits the detailed examination and modeling of diffraction data without explicit knowledge of the area S. A complete development of the relative absolute scale is given by Jacobs and White (1989) (see in particular eqs 2–4). Summarizing briefly here, the relative absolute scale $\rho^*(z)$ is given by the absolute density $\rho(z)$ multiplied by the area S. The relative absolute density $\rho^*(z)$ is in units of scattering length (or electrons) per unit length, which are the appropriate dimensions for describing the structure determined from lamellar (one-dimensional) diffraction. In addition, the relative absolute scale is determined on a per lipid molecule basis so that the average density $\rho_0 \cdot S = \rho_0^*$ is determined directly from knowledge of the contents of the half-bilayer unit cell, which consists of the lipid molecule and its associated waters of hydration. This places the profiles on the true zero of relative absolute scattering space. The Fourier cosine series generated from a set of measured structure factors $f(h)$, which is the arbitrary scale density profile typically presented in membrane diffraction papers, describes the fluctuations in density about the average density ρ_0^*. However, these measured structure factors $f(h)$ are related by an arbitrary experimental scale factor k to the desired relative absolute structure factors $F^*(h)$, i.e., $f(h)/k = F^*(h)$. Therefore, determination of relative absolute profiles requires knowledge of the unit cell contents and determination of the instrumental constant k. In our X-ray diffraction setup, the measured diffraction intensities vary from experiment to experiment because of variations in X-ray tube performance and the amount of sample in the beam. The result is that each experiment has a different scale factor, which complicates the analysis. Existing methods for the analysis of diffraction data from centrosymmetric isomorphous structures (Hargreaves, 1957; Zaccai et al., 1975; Worcester & Franks, 1976; Büldt et al., 1979) consider all of the data to have the same scale factor, so it was necessary to develop a generalized method for treating diffraction from mixtures with different scale factors. This method is described in the Appendix. Subsequent profiles will be presented on the relative absolute scale in units of scattering length per unit length. We stress the importance of scaling the data for two primary reasons. First, for the eventual joint refinement of neutron and X-ray diffraction data, accurate relative absolute structure factors are essential. Incidentally, we use scattering length instead of electrons to describe X-ray diffraction data because neutron scattering is expressed conventionally in scattering length units; X-ray scattering length can be converted to electrons by dividing by the factor e^2/mc^2 (Warren, 1969). Second, the correct scaling yields the most informative structural images of the bilayer that will provide the most insight into the actual packing within membranes.

X-ray Phase Determination. The phases of the X-ray structure factors were determined with a method described by Franks et al. (1978). If the bromine distribution in OBPC can be considered as a Gaussian distribution, then the structure factors $F_{Br}(h)$ that arise from it are given analytically by

$$F_{Br}(h) = 2b_{Br} \exp[-(\pi A_{Br} h/d)^2] \cos(2\pi h Z_{Br}) \quad (2)$$

where b_{Br} is the scattering length of the two bromine atoms in OBPC, A_{Br} is the $1/e$ half width of the Gaussian, and Z_{Br}

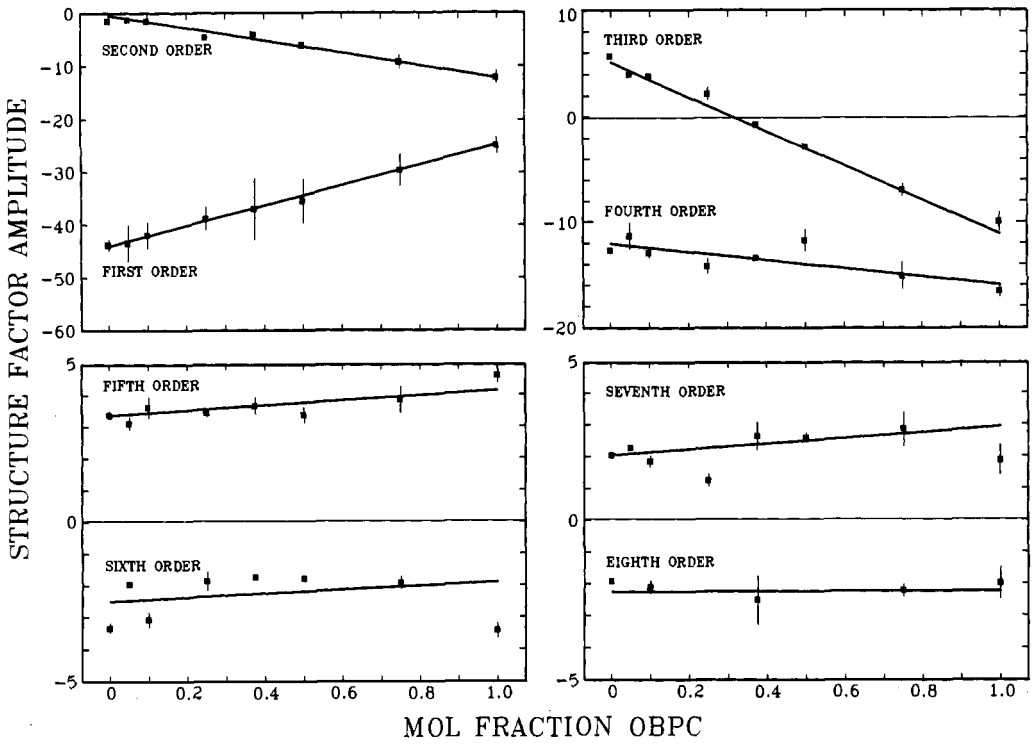

FIGURE 3: Relative absolute structure factors $F^*_x(h)$ vs mole fraction x of OBPC for a series of eight OBPC/DOPC mixtures. The data were analyzed by using the formalism described in the Appendix. Individual points are the relative absolute structure factors that are related to the measured structure factors by instrumental scale factors. The error bars are obtained from the uncertainties in the values of integrated intensities measured from the X-ray films. The solid lines show the best values of the absolute structure factors based upon a self-consistent fit of all of the data (cf. Appendix).

is its center. All of the terms except the cosine factor are positive-definite, but the sign of the cosine term will vary depending upon the value of h and, importantly, the center Z_{Br} of the bromine distribution. Selecting a value of Z_{Br} then leads to prediction of the signs and magnitudes of $F_{Br}(h)$, which in turn indicates the changes in the values of the structure factors of mixtures containing different amounts of bromine. If the data sets at different bromolipid mole fractions x are phased correctly, then for each value of h the graph of structure factor $F_x(h)$ versus x should be linear and the slope of the line should be in a direction consistent with the choice of Z_{Br}. The resultant difference structure factors between a mixture of mole fraction x and pure DOPC will then describe the distribution of bromines within the bilayer. A Gaussian function is fit in reciprocal space to these difference structure factors, and the center Z_{Br} of this calculated Gaussian can now be inserted into eq 2 as a consistency check to make sure that the structure factors of the mixtures change in a direction consistent with the calculated value of Z_{Br}.

Results

At 66% RH, pure OBPC and pure DOPC each form bilayers with similar repeat periods of $d = 50.2 \pm 0.3$ and 49.1 ± 0.3 Å, respectively. Both display a broad wide-angle diffraction peak centered at 4.5 Å that is characteristic of the liquid-crystalline L_α phase (Small, 1986). All of the calculated results to be presented are based upon a single d-spacing value of 49.1 Å for all of the mixtures. The treatment of data with different d-spacings can be accommodated by a correction factor used to scale data sets from swelling experiments (Blaurock, 1971). For OBPC and DOPC, this correction, on the order of 1% for the observed difference in d-spacing of 1 Å, was omitted. The widths of the lamellar diffraction peaks were nearly constant with increasing h, which indicates that all of the mixtures formed well-ordered one-dimensional lattices (Wiener & White, 1991a). Structure factors were determined from experiments performed on oriented samples prepared from eight different OBPC/DOPC mixtures containing 0.00, 0.05, 0.10, 0.25, 0.375, 0.50, 0.75, and 1.00 mole fraction OBPC.

Figure 3 shows the variation with mole fraction x of OBPC of the relative absolute structure factors $F^*_x(h)$ after determination of the instrumental constant k_x for each OBPC/DOPC mixture. The solid lines depict the best determinations of the values of the relative absolute structure factors as a function of the mole fraction of OBPC. Note that all eight of the lines (one for each order) are coupled by the requirement that all of the structure factors from a given mole fraction x must have the same scale factor. The data are analyzed with a global multiple linear regression method, detailed in the Appendix, that calculates the best set of instrumental scale factors k_x and places all of the data on the relative absolute scale. In this analysis the error function that is minimized during the fitting is essentially the sum of the squares of the differences between the data points of a given order and its fitted line *summed over all of the orders*. Therefore, the line that describes the best relative absolute structure factors for each order h is not necessarily equal to the best independent linear fit of the data for that order.

Inspection of Figure 3 shows that the lines, particularly for the largest amplitude structure factors, pass through most of the data points and are very similar to the best linear fits of data at individual orders. The data points are farther away from the solid lines for the higher orders reflecting the fact that it is difficult to observe the higher order intensities and to determine accurate structure factors from them. The error bars for each data point, based upon variation in the value of the integrated intensity observed for each order, are included for comparison although they were not used to weight the data in the actual calculation. These experimental uncertainties

were not used for weighting because it was unclear whether there were enough determinations of each data point for the uncertainties to provide meaningful estimates of structure factor accuracy. Inspection of Figure 3 indicates that the estimated errors of higher orders are probably too low. This observation highlights a virtue of the global analysis method. Acquiring a complete set of diffraction data at a given mole fraction is fairly arduous, and determining all of the structure factors to high accuracy is particularly daunting. Because the equations for determining the instrumental scale factors are highly overdetermined by the experimental data, the consistency of the results obtained with data over a wide range of concentrations serves as an excellent assay of the quality of experimental data. The distance of a data point from the line is a reasonable measure of its error especially in comparison with uncertainties estimated from a single experiment. The results of Figure 3 are completely consistent with the expectation that the larger amplitude structure factors corresponding to lower orders can be measured more accurately than the small higher order structure factors.

The signs of the slopes of the lines for orders $h = 1-7$ in Figure 3 are consistent with the signs determined from eq 2 with the value of Z_{Br} that was determined from fitting a Gaussian to the difference structure factors (vide infra). The lines are also consistent with the phases of the structure factors of DOPC determined by sampling theorem analysis (Shannon, 1949; Franks, 1976) of swelling experiments (data not shown). For the eighth order, a negative slope is predicted while a positive slope is actually observed. If the analysis is repeated with the phase of the eighth order changed from -1 to $+1$, the sign of the slope is consistent with the sign determined from the value of Z_{Br}. We used several additional criteria to resolve this ambiguity and decided upon an eighth order phase of -1 as shown in Figure 3. First, because the solid lines in Figure 3 are close to the best linear least-squares fits at each order, the uncertainty in the slope of the line at the eighth order can be estimated by linear least-squares methods. The calculated slope and its uncertainty are -0.01 ± 0.55 so a positive slope is well within the error of the experimental uncertainty of the eighth order data. The value of the slope is expected to be close to zero as the $1/e$ half-width of the bromine Gaussian distribution exponentially reduces the magnitude of its structure factors with increasing order (eq 2) so that the eighth order structure factor changes very little with increasing amounts of OBPC. The higher order structure factors are very difficult to measure accurately, and this is reflected in the uncertainty of the slope being much larger than the value of the slope. Therefore, within experimental error an eighth order phase of -1 is consistent with the analysis. The alternate choice of an eighth order phase of $+1$ was eliminated by an examination of Fourier density profiles of DOPC/OBPC mixtures calculated with this phase value. Profiles (including pure DOPC) with a positive eighth order displayed terminal methyl regions with broad flat minima, and each methyl trough minimum had a slight positive feature in its center (data not shown). This feature is inconsistent with existing images of the terminal methyl distribution in fluid bilayers [for example, Levine and Wilkins (1971), Torbet and Wilkins (1976), and McIntosh and Simon (1986)], so this phase choice was eliminated. We note also that the eighth order phase could not be determined unambiguously from continuous transforms calculated from DOPC swelling data (data not shown). Just as we utilized existing structural information to rule out a phase choice, additional physicochemical information is often utilized to resolved ambiguity in phase assignments from

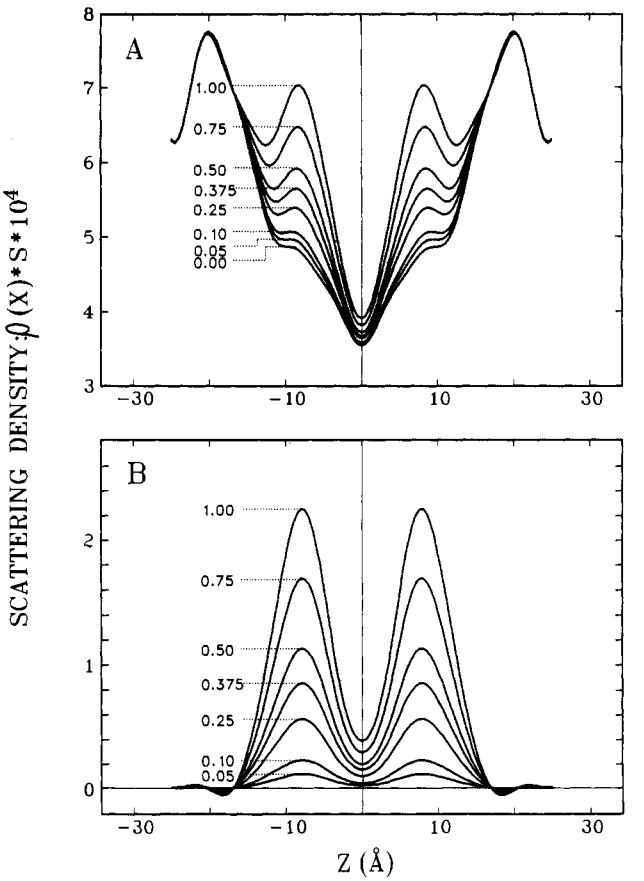

FIGURE 4: Relative absolute scattering density profiles of OBPC/DOPC bilayers and difference bromine profiles. (A) Eight-order Fourier profiles of the eight OBPC/DOPC mixtures: 0.00, 0.05, 0.10, 0.25, 0.375, 0.50, 0.75, and 1.00 mole fraction OBPC. The absolute structure factors used to calculate the profiles are taken from the solid lines in Figure 3. The profiles are strikingly similar in the headgroup region. A peak localized at ≈8 Å is seen to increase with increasing amounts of OBPC and is readily identified as the distribution of the bromine atoms covalently attached at the 9 and 10 positions of the 2-chain. (B) Difference Fourier profiles between each of the OBPC-containing mixtures and pure DOPC. The monotonic increase in the peak with increasing OBPC content is apparent.

continuous transforms (Torbet & Wilkins, 1976; Franks, 1976).

The eight-order Fourier density profiles of the eight OBPC/DOPC mixtures are shown in Figure 4A. The relative absolute structure factors for each mole fraction are taken from the solid lines of Figure 3. The hydration number of DOPC at 66% RH has been previously determined (White et al., 1987; White & Jacobs, 1989) so that the profiles can be placed on the relative absolute scale in units of scattering length/unit length vs position. The similarity in the headgroup region among all of the mixtures is striking. The peaks located ≈8 Å from the bilayer center, which steadily rise with increasing OBPC concentration, are clearly identifiable as the increase in scattering from the bromine atoms at the 9 and 10 positions of the 2-chain. Figure 4B depicts the difference Fourier profiles between each of the mixtures containing OBPC and pure DOPC. The transbilayer bromine distribution is described very well by a pair of Gaussians equidistant from the center of the bilayer. The position Z_{Br} and $1/e$ half-width A_{Br} of the Gaussian were determined by fitting eq 2 to the relative absolute difference structure factors with nonlinear minimization of the crystallographic R factor (Wiener & White, 1991b) rather than of the usual least-squares merit function. The distribution of bromines in OBPC/DOPC bilayers at 66% RH is described by a pair of Gaussians each at a distance Z_{Br}

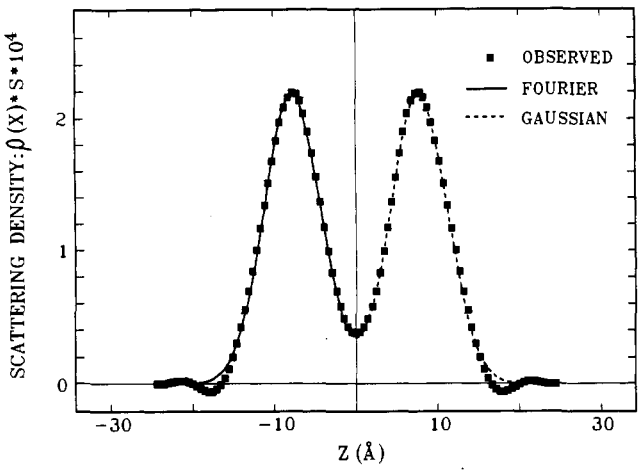

FIGURE 5: Comparison of a bromine difference profile and its Gaussian fit. The squares depict the eight-order Fourier profile generated from the difference structure factors between 1.00 mole fraction OBPC and pure DOPC and is identical with the profile labeled 1.00 in Figure 4B. The right half of the figure compares this profile to the Gaussian function fit in reciprocal space to these difference structure factors. The left half of the figure compares the profile to the eight-order reconstruction of the fitted Gaussian. The fitted Gaussians are each 7.97 ± 0.27 Å from the center of the bilayer with $1/e$ half-widths of 4.96 ± 0.62 Å. A comparison of the data and fitted Gaussian reveals that the fully resolved transbilayer distribution of bromine atoms is accurately represented by a pair of Gaussian functions.

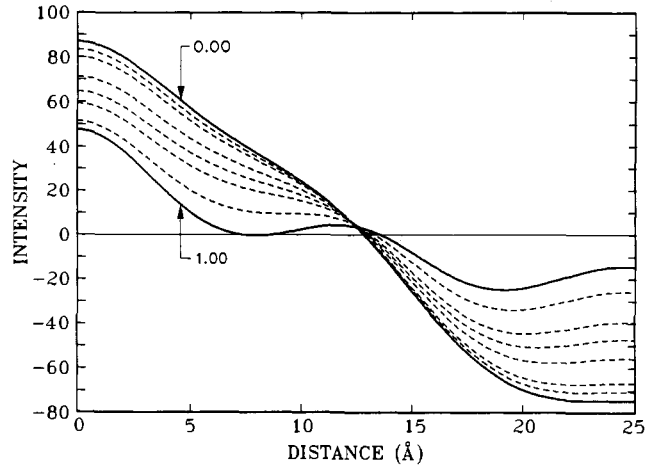

FIGURE 6: One-dimensional Patterson maps of the OBPC/DOPC mixtures. The profile of 1.00 mole fraction OBPC has a discernible peak at ≈12 Å that corresponds to the separation between the bromine label and the phosphate moiety of the headgroup. While a clear peak is not seen in any of the other profiles, they all intersect approximately at the position corresponding to the distance between the bromines and/or double bonds and the phosphate, and the derivative of each profile has an inflection point at this position.

= 7.97 ± 0.27 Å from the bilayer center with a $1/e$ half-width A_{Br} = 4.96 ± 0.62 Å. The eight-order profile of this fitted Gaussian as well as the fitted Gaussian itself is compared to the experimental difference profile between 1.00 mole fraction OBPC and DOPC in Figure 5. All of the difference profiles have the same Gaussian envelope and are merely scaled by the total amount of bromine in each mixture. The uncertainties in the Gaussian parameters were determined by a Monte Carlo sampling procedure (Press et al., 1989). Each value of a structure factor and its associated error are used to define a normal distribution. Sets of mock data are generated by random sampling from these normal distributions, and the scaling (see Appendix) and Gaussian fitting calculations are repeated with each new "noisy" data set as input. The results of N = 100 iterations were averaged, and the standard deviations of Z_{Br} and A_{Br} from this simulation serve as estimates of the parameter uncertainties.

A one-dimensional Patterson map can be calculated from lamellar diffraction intensities by a formula analogous to that used to calculate Fourier density profiles (Worthington, 1969).

$$P(z) = (2/d)\sum_{h=1}^{h_{max}} |F(h)|^2 \cos(2\pi hz/d) \qquad (3)$$

The position of a peak in the Patterson map is the distance between a pair of significant scattering regions in the half bilayer unit cell. The one-dimensional Patterson functions of each of the OBPC/DOPC mixtures are shown in Figure 6. The profile of 1.00 mol fraction OBPC shows a peak at ≈12 Å that corresponds to the distance between the bromine label and the phosphate moiety. This separation is consistent with the distance between Z_{Br} (7.97 ± 0.27 Å) and the phosphate peak (≈20 Å as seen in Figure 4A). While no discernible peaks are observable in any of the other OBPC/DOPC mixtures, the series of Patterson maps all intersect at approximately the same position (≈12 Å). Starting with pure DOPC, increasing amounts of OBPC have the apparent effect of rotating the Patterson profiles counterclockwise until the 12-Å feature in pure OBPC is a clear peak. It is interesting that each of the profiles, including DOPC, has a noticeable change in slope at a position corresponding to this distance between the positions of the phosphate and bromines (and/or double bonds). Specifically, the derivative of each Patterson map has an inflection point at about 12 Å.

Discussion

X-ray diffraction analysis of a series of OBPC/DOPC mixtures has provided a fully resolved image of the distribution of bromines in a specifically halogenated lipid. Inspection of the Fourier profiles of the OBPC/DOPC mixtures (Figure 4A) indicates that OBPC is an excellent structural isomorph for DOPC under the experimental conditions of this study. The bromine distribution is localized within the bilayer at a position Z_{Br} = 7.97 ± 0.27 Å that is similar to the position of the C9–C10 double-bond distribution of DOPC as determined from neutron diffraction of DOPC specifically deuterated at the double bond (Jacobs & White, 1989; Wiener et al., 1991). To a very good approximation, OBPC can be viewed as DOPC with an additional bromine distribution added at the double-bonded region. We stress that the bromine distribution is a fully resolved image (Wiener & White, 1991a) of a membrane component located within the bilayer interior. The position of the bromine is also reliably obtained from an inspection of the one-dimensional Patterson map of pure OBPC (Figure 6), which indicates the possibility of using this phase-invariant method to obtain an accurate determination of the position of a halogen or other significantly scattering label within a bilayer. Our results on the isomorphous nature of specific bromination are in general agreement with previous X-ray diffraction results of McIntosh and Holloway (1987) on a series of 1-palmitoyl-2-dibromostearoyl-*sn*-glycero-3-phosphocholines brominated at various positions along the 2-chain. By a comparison of the continuous transforms of specifically brominated and nonbrominated lipids obtained from swelling experiments, they demonstrated that the structures of bromolipids labeled at the 6,7- and 11,12-positions could each be adequately approximated by the sum of the structure of 1-palmitoyl-2-oleoyl-*sn*-glycero-3-phosphocholine and a pair of Gaussians, equidistant from the bilayer center with $1/e$ half-widths of 4 Å, that represented the bromine atoms. Their results are based upon trial-and-error fitting of

Gaussian functions to five or six orders of diffraction data and thus probably do not provide fully resolved images of the bromine labels. Also, in their experiments on unoriented bilayers, higher order structure factors are especially difficult to measure because the observed intensity of an ordered h is reduced by a Lorentz factor of h^{-2} instead of the factor h^{-1} in our oriented samples. However, the overall agreement of our results obtained from oriented bilayers at 66% RH with their results an unoriented bilayers in excess water is encouraging.

It is of interest to examine the influence of the size of the bromine atoms upon the observed width of the bromine distribution. The image of the bromine atoms across the bilayer can be represented as the convolution of two distributions: the hard-sphere or van der Waals stationary distribution of the bromine atoms and an envelope of thermal motion. For this simple calculation, consider each of these distributions, hard-sphere and thermal, to be represented by Gaussian distributions of $1/e$ half-widths A_H and A_T, respectively. While the hard-sphere distribution is more commonly represented by a strip, use of a strip needlessly complicates the calculation and adds little to the essential result; also, most of the total molecular area (85%) of the hard-sphere distribution is enclosed within the region spanned by $\pm A_H$ from the center of the Gaussian. The convolution product of two Gaussians is another Gaussian of $1/e$ half-width $(A_H^2 + A_T^2)^{1/2}$ (Hosemann & Bagchi, 1962). A value of $A_H \approx 3.0$ Å, obtained from values of covalent bond lengths and van der Waals radii (Pauling, 1960), yields a thermal envelope with a $1/e$ half-width $A_T \approx 3.9$ Å. The high degree of thermal disorder in liquid-crystalline bilayers (Wiener & White, 1991a) is reflected in this value of A_T.

An example of an application of X-ray diffraction to the interpretation of fluorescence quenching experiments is given by a consideration of the "parallax" method of Chattopadhyay and London (1987). Their approach uses the ratio of fluorescence quenching obtained from separate experiments on mixtures with quenchers at different positions within the bilayer to obtain the position of a fluorophore within the bilayer. Determining an accurate fluorophore position requires prior estimates of the quenchers' positions within the bilayer because these positions are used directly in the formulas used to determine fluorophore position (Chattopadhyay & London, 1987). While the amounts of quencher typically used in fluorescence experiments are much smaller than those detectable by X-ray diffraction, the isomorphous behavior of OBPC indicates that the position of the bromine is invariant with mole fraction. Therefore the positions obtained from X-ray diffraction can be used directly as input into the distance calculations. In this context, Abrams and London (1991) have recently presented results on the calibration of their parallax method (Chattopadhyay & London, 1987) by the use of bromolipids characterized by McIntosh and Holloway (1987). While our results are for oriented bilayers at moderate hydration, similar studies could be conducted on multilamellar vesicles in excess water, which is a system more similar to that used in fluorescence experiments. Solution scattering of unilamellar vesicles may also yield the phosphate–quencher separation. It may also be possible to determine fluorophore positions and thus provide a complete check of the method, i.e., the positions of fluorophores and quenchers can be used to back-calculate fluorescence quenching ratios for comparison to experiment.

In addition to average position, X-ray diffraction can yield the fully resolved image of the transbilayer distribution of a quencher (and possibly a fluorophore also). This information raises the possibility of further refinement of the theories used to interpret quenching data that conventionally treat the fluorophore and quencher as point particles. A more realistic treatment incorporating the accurate distribution functions obtained from diffraction could influence the interpretation of data. Examination of the OBPC bilayer distribution in Figure 4B indicates that the bromine has a significant probability of occupying any position within the hydrocarbon interior of the bilayer. Therefore, the likelihood of an excited fluorophore *anywhere* in the bilayer interior being quenched is greater than if one considered the quencher as a point particle anchored at a single position. A more detailed and realistic theory could utilize overlap integrals of fluorophore and quencher probability distributions to fit quenching data. Also, one theory of static quenching (Perrin, 1924; Chattopadhyay & London, 1987) considers the quencher to have a characteristic sphere or disc of influence within which all excited fluorophores are quenched. Quencher (and fluorophore) distributions obtained by diffraction methods in conjunction with fluorescence quenching data could possibly relate this "quenching distance" directly to physicochemical properties of the membrane.

X-ray diffraction holds considerable promise as a method for determining the positions and distributions of halogen labels in membranes. Several strategies for diffraction experiments are envisioned. For example, if the label on a phospholipid contributes significantly to the total scattering, then Patterson methods could be used to locate the label. The bromine in OBPC contributed about 20% of the total scattering of pure OBPC bilayers and gave rise to a discernible peak in the Patterson map (Figure 6) that corresponded to the phosphate–bromine separation. A more detailed investigation of a series of mixtures by the methods described in the Appendix can yield a fully resolved image of a transbilayer label distribution particularly if the distribution is well represented by a Gaussian function. A simple Gaussian distribution also makes the determination of the most consistent phase angles straightforward. Typically, analysis of swelling curves by continuous transform methods is used to determine phases; however, phasing higher order structure factors in this way is not trivial. Also, the d-spacing of many bilayers, such as DOPC, does not vary appreciably with hydration, and this further complicates the use of swelling experiments for phasing. Specific labeling methods can complement swelling experiments for phase determination and may perhaps be as reliable or even more reliable than swelling methods under some circumstances. Lastly, the extension of membrane X-ray diffraction techniques to other membrane components, i.e., peptides, proteins, and other solutes, is envisioned as a panoply

Table I: Positions Z, $1/e$ Half-Widths A, and Crystallographic R Factors for Gaussian Fits of Transbilayer Bromine Distributions Based upon Experimental Difference Structure Factors between OBPC/DOPC Mixtures Containing a Mole Fraction x of OBPC and Pure DOPC[a]

x	Z	A	R
0.05	7.81	4.75	0.2070
0.10	7.20	4.50	0.1084
0.25	7.88	4.96	0.0530
0.375	7.74	5.03	0.0638
0.50	8.18	5.34	0.0700
0.75	7.89	4.96	0.0247
1.00	7.98	5.01	0.0115
	7.81 ± 0.30[b]	4.94 ± 0.26[b]	0.0769 ± 0.0655[b]

[a] The units for Z and A are ångströms. [b] Mean values and standard deviations of Z, A, and R.

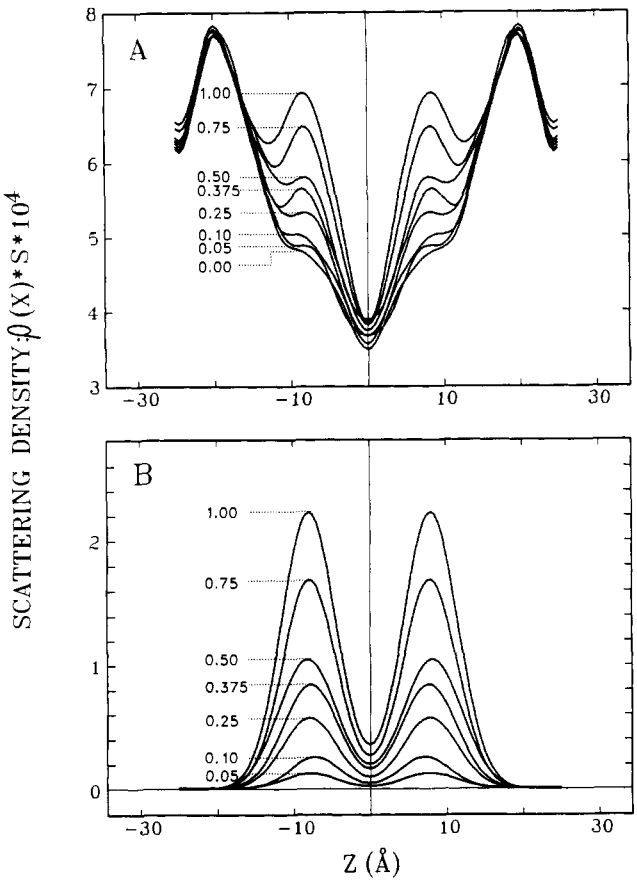

FIGURE 7: Relative absolute scattering density profile of OBPC/DOPC bilayers and difference bromine profiles based upon scaled experimental structure factors (the data points in Figure 3). (A) Eight-order Fourier profiles of the eight OBPC/DOPC mixtures: 0.00, 0.05, 0.10, 0.25, 0.375, 0.50, 0.75, and 1.00 mole fraction OBPC. (B) Gaussian distributions fit to the experimental difference structure factors between each of the OBPC-containing mixtures and pure DOPC.

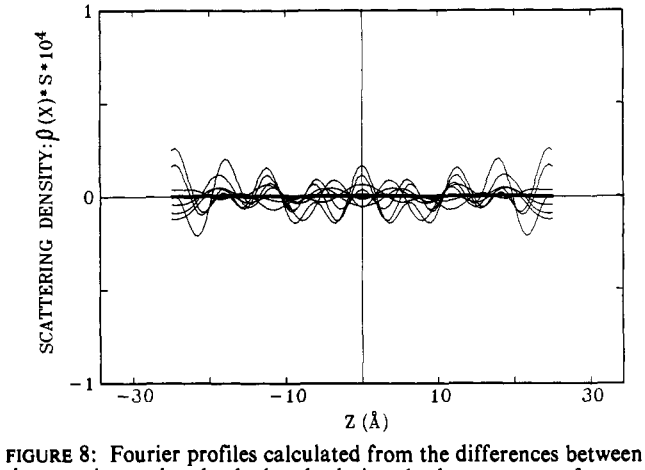

FIGURE 8: Fourier profiles calculated from the differences between the experimental and calculated relative absolute structure factors. The heavy line is the average of all of the profiles.

of methods exist for the chemical modification of amino acids (Lundblad & Noyes, 1984).

ACKNOWLEDGMENTS

We gratefully acknowledge Prof. Kenneth J. Longmuir for providing expert technical assistance on lipid synthesis and HPLC of phenacyl esters and Ms. Sherry Haynes for assistance with the phosphorus assays. We also acknowledge useful discussion with Profs. P. W. Holloway, J. R. Silvius, and E. A. Dawidowicz regarding specific bromination of lipids.

APPENDIX

Scaling Multiple Data Sets. Consider a two-component bilayer composed of molecules A and B that are nearly identical except for a few atoms that have large differences in scattering length. If the two molecules are isomorphous, then bilayers formed from mixtures of A and B can be described by the mole fraction weighted combination of the structures of pure A and pure B. The relative absolute structure factors $F_x^*(h)$ of a mixture containing a mole fraction x of molecule A will be given by

$$F^*_x(h) = xF^*_A(h) + (1 - x)F^*_B(h) \quad \text{(A1)}$$

where $F_0^*(h) = F_B^*(h)$ and $F_1^*(h) = F_A^*(h)$. If one could measure $F_A^*(h)$ and $F_B^*(h)$, then the structure factors of all A/B mixtures can be predicted. However, $F_A^*(h)$ and $F_B^*(h)$ are not measured directly in diffraction experiments. Experiments yield sets of structure factors $f_x(h)$ that are related to $F^*_x(h)$ by instrumental scaling constants k_x (King et al., 1985; Jacobs & White, 1989; Wiener & White, 1991b)

$$f_x(h) = k_xF^*_x(h) \quad \text{(A2)}$$

The scale factor k_x has no physical connection to the bilayer structure but is related solely to the experimental setup. Experimental factors affecting k_x include (a) the sample-beam intersection, (b) the exposure time and film processing conditions, (c) the amount of sample on the glass substrate, and (d) the incident beam intensity. Rewriting eq A1 in terms of the observed structure factors,

$$f_x(h)/k_x = xf_A(h)/k_A + (1 - x)f_B(h)/k_B \quad \text{(A3)}$$

Given two sets of measured structure factors $f_A(h)$ and $f_B(h)$, the scale factors k_A and k_B can be determined by relating the structures of A and B to absolute scattering space through a comparison of their relative absolute Fourier density profiles. The relative absolute profiles $\rho^*_j(z)$ are given by (Jacobs & White, 1989; Wiener & White, 1991b)

$$\rho^*_j(z) = \rho^*_{oj} + (2/dk_j)\sum_{h=1}^{h_{max}} f_j(h) \cos(2\pi hz/d) \quad \text{(A4)}$$

The first term on the right-hand side of the equation, ρ^*_{oj}, is the average density per unit length of the bilayer. The second term describes the fluctuations in scattering length about this average across the bilayer, and the subscript j denotes molecule A or B. At a point $z = z_1$ where the two profiles are identical, $\rho^*_A(z) = \rho^*_B(z)$ and

$$(2/dk_A)\sum_{h=1}^{h_{max}} f_A(h) \cos(2\pi hz_1/d) - (2/dk_B)\sum_{h=1}^{h_{max}} f_B(h) \cos(2\pi hz_1/d) = \rho^*_{oB} - \rho^*_{oA} = \Delta\rho^* \quad \text{(A5)}$$

If the difference $\Delta\rho^*$ in average densities of the two samples is known, two "matchpoints" z_1 and z_2 are sufficient to determine k_A and k_B, which yields the relative absolute structure factors $F^*_A(h)$ and $F^*_B(h)$.

The analysis becomes more complicated if a larger number of data sets over a range of mole fraction x are utilized instead of data solely from pure A and pure B bilayers. If each experiment were performed and analyzed under completely invariant conditions, then a single scale factor k_x would suffice to place all of the data on the relative absolute scale. However, conditions, particular beam intensity and the amount of sample in the beam, change from experiment to experiment so that each data set at a different mole fraction has a different scale

factor k_x. The scale factors k_x can be calculated by solving the set of h_{max} linear equations, one for each diffraction order 1, 2, 3, ..., h_{max}, which are represented by eq A3. For a single mole fraction x, there are $2h_{max} + 1$ unknown parameters, the relative absolute structure factors $F^*_A(h) = f_A(h)/k_A$ and $F^*_B(h) = f_B(h)/k_B$ (h_{max} each), and the scale factor k_x, so the system of equations is underdetermined. However, each additional set of structure factors obtained from a sample at a different mole fraction adds another h_{max} independent equations but only *one* additional unknown, the scale factor k_x for that particular mole fraction. For $h_{max} \geq 3$, satisfied by virtually all fluid bilayers, structure factors determined at three different mole fractions are sufficient to obtain values of $F^*_A(h)$, $F^*_B(h)$, and the three instrumental scale factors k_x. Preferably, as in this paper, more than three mixtures are examined; the system of equations is then overdetermined, and multiple linear regression can be used to find an optimized solution set.

Inspection of eq A3 reveals an additional complication. Rearranging the terms of eq A3 shows explicitly that the set of linear equations that define the scaling are homogeneous

$$f_x(h)/k_x - xf_A(h)/k_A - (1 - x)f_B(h)/k_B = 0 \quad (A6)$$

so that $F^*_A(h) = f_A(h)/k_A$, $F^*_B(h) = f_B(h)/k_B$, and k_x are not uniquely determinable. Each set of equations for a given mole fraction x can be multiplied by a different arbitrary constant c_i:

$$c_i f_x(h)/k_x - c_i x f_A(h)/k_A - c_i(1 - x)f_B(h)/k_B = 0 \quad (A7)$$

The solution of eq A7 yields a set of normalization constants $c_i/k_x \equiv 1/k^\dagger_x$ that place all of the observed structure factors $f_x(h)$ on an internally consistent linear scale. Instead of a set of instrumental scale factors k_x that relate $f_x(h)$ to $f_A(h)/k_A$ and $f_B(h)/k_B$ (eq A3), the normalization factors $k^\dagger_x$ in eq A7 relate $f_x(h)$ to a "basis set" of structure factors $f^\dagger_A(h)/k_A$ and $f^\dagger_B(h)/k_B$, where $f^\dagger_A(h)$ and $f^\dagger_B(h)$ are linear functions of the arbitrary constants c_i:

$$f_x(h)/k^\dagger_x = xf^\dagger_A(h)/k_A + (1 - x)f^\dagger_B(h)/k_B \quad (A8)$$

Solving eq A8 places the data on a self-consistent internally normalized scale that is necessary but not sufficient to solve the scaling problem. The data remain on an essentially arbitrary scale because they have not yet been connected in any specific way to the absolute structure of the bilayer. However, we are now at exactly the same stage as in the analysis of two sets of data from pure A and pure B. With $f^\dagger_A(h)$ and $f^\dagger_B(h)$ as input into eq A5, k_A and k_B are calculated and the relative absolute structure factors $F^*_A(h)$ and $F^*_B(h)$ are determined. Equation A3 is now inhomogeneous [$f_A(h)/k_A = F^*_A(h)$ and $f_B(h)/k_B = F^*_B(h)$ are fixed], so its solution yields a unique set of instrumental scale factors k_x that places all of the data $f_x(h)$ on the correct relative absolute scale.

In practice, the structure factor plots (Figure 3) and Fourier profiles (Figure 4) should be examined carefully to check the consistency of the analysis. If many of the $F^*_x(h)$ values are not colinear, then the selection of matchpoints or choice of phases could be flawed. Inspection of the Fourier profiles can reveal anomalous behavior that could arise from forcing the two structures to agree at incorrect matchpoints. If small shifts in the matchpoints yield large fluctuations in k_A and k_B, then their selection is likely to be incorrect. Ideally, as in the case of OBPC/DOPC mixtures, there is close agreement of the profiles over a wide enough range (Figure 4A) so that (i) the solution is robust, i.e., k_A and k_B are constant over a range of matchpoints, and (ii) the two matchpoints can be separated enough to generate two nonsingular equations for determining k_A and k_B. The values $d/2$ and 20.0 Å were used as the two matchpoints for OBPC and DOPC. Because OBPC is a good isomorph for DOPC (Figure 4A) with close agreement in much of the headgroup region, the results were affected negligibly by the choice of matchpoints as long as they were between ≈18 Å and $d/2$.

Discussion. The best estimates of the relative absolute structure factors $F^*_x(h)$ obtained from the fitted curves of the global analysis (the solid lines of Figure 3) were used for the determination of the bromine distribution in OBPC/DOPC bilayers reported in the body of this paper. It is of interest to compare the bilayer profiles and bromine distributions obtained from these fits (Figure 4) to similar profiles (Figure 7) obtained directly from the scaled experimental data (the data points of Figure 3). Compared to Figure 4A, the set of OBPC/DOPC profiles in Figure 7A do not overlap as completely in the headgroup region and the positions of the bromine distributions are not as closely aligned. However, there are no systematic differences between the two families of profiles. In both figures, the size of the bromine distribution increases monotonically with OBPC concentration, and the position of the peak is nearly constant. The peak in the 0.05 mole fraction is difficult to resolve because the bromine scattering contributed by this amount of OBPC is at our limit of detection.

Figure 7B shows the Gaussian distributions fit to each of the seven sets of experimental difference structure factors. Comparing this figure to Figure 4B again demonstrates that, while experimental noise shifts the positions and widths of the distributions a small amount, the two families of distributions are entirely consistent. The parameters of each of the fits shown in Figure 7B are listed in Table I. As the mole fraction of OBPC increases, the quality of the Gaussian fit improves because the difference structure factors become larger relative to the experimental noise of the data sets that they are calculated from. Likewise, if only two data sets are used for scaling, increasing the difference between their average densities ($\Delta\rho^*$ in eq A5) will decrease the uncertainty in the determination of the scale factors k_A and k_B. The average position Z_{Br} and $1/e$ half-width A_{Br} of the Gaussians in Figure 7B are 7.81 ± 0.30 and 4.94 ± 0.26 Å, respectively. The uncertainties in the Gaussian parameters reflect the variation among different pairs of data sets but do not include the effect of the uncertainty of individual data points upon the determination of the bromine distribution. This error can be estimated by Monte Carlo simulation (vide supra). The Gaussian parameters and simulated errors of the complete analysis are Z_{Br} = 7.97 ± 0.27 Å and A_{Br} = 4.96 ± 0.62 Å. These are in excellent agreement with the results in Table I. In addition, the average R factor of the Gaussian fits in Table I, R = 0.0769, is comparable with the experimental precision of the data.

Another way to compare the experimental and optimized data is to examine the density profiles calculated from the differences between the scaled experimental structure factors and the scaled optimized structure factors. The amplitude of this difference profile provides a measure of the overall "goodness of fit" between two sets of structure factors, and its periodicity reveals which orders of the two data sets have the largest differences. If the global analysis were actually suppressing some nonisomorphous structural features, then these difference profiles would be expected to show this feature and its magnitude would increase systematically with increasing OBPC concentration. As seen in Figure 8, there is no apparent systematic variation in the profiles with increasing

amounts of OBPC. The periodicity indicates that, as discussed earlier, the higher order structure factors have the largest errors, so they will deviate the most from the best values obtained in the global analysis. The heavy line shows the average of all of the profiles, which is virtually zero across the bilayer. Except for the transbilayer Guassian distribution of bromine atoms, there is no observable perturbation of DOPC by OBPC that we can distinguish from experimental noise.

One does not know a priori that two molecules A and B form an isomorphous replacement pair. Mixtures of two molecules may only be isomorphous over a limited range of composition, and this range can be determined by experiments at different mole fractions. Even if the two molecules are eventually shown to be good isomorphs, as in the case of OBPC and DOPC, an important advantage is the improved accuracy and better statistics obtained from simultaneously analyzing data from more than two mixtures. Using only the measured structure factors $f_A(h)$ and $f_B(h)$ places stringent demands upon their accuracy. The cosine factor in eq A5 implies that different structure factors will be weighted differently depending upon the choice of matchpoints. It is possible that the smaller higher order structure factors, which are the most difficult to measure accurately, could dominate the calculation of scale factors and introduce large uncertainties. The two situations (two data sets versus many data sets) can be compared to fitting a straight line to two or more than two points; more than two points is clearly preferable.

We have shown that OBPC is an excellent structural isomorph for DOPC under the conditions of this study, i.e., the observed structure of a OBPC/DOPC mixture is described very well by the mole fraction weighted sum of the individual structures of OBPC and DOPC (eq A1). Equation A1 can be viewed as a requirement for ideal mixing of a two component bilayer. Is this requirement of ideal mixing only valid for mixtures of two molecules A and B that are structural isomorphs? While strict isomorphous behavior is not required, "complementarity" of the structures of A and B is required such that each molecule does not perturb the long-time average packing of the other. This complementarity is most readily associated with structural isomorphs, but one can speculate on other possibilities. Perhaps a mixture of lipids and transmembrane peptides can be described as the mole fraction weighted sum of lipid and peptide structures. Another possibility is that complementarity is maintained over a subset of the full 0.00–1.00 mole fraction range so that the analysis can be conducted over this limited range. Another factor is that as two structures deviate from isomorphous behavior their difference profile becomes more complex, so that it becomes more complicated to use this difference profile to phase the data. A simple localized distribution, as in the case of the bromines of OBPC, is very well described by a Gaussian, so that the phasing approach of Franks et al. (1978) works exceedingly well.

Registry No. OBPC, 120246-71-1; DOPC, 4235-95-4; bromine, 7726-95-6.

References

Abrams, F., & London, E. (1991) *Biophys. J. 59*, 629a.

Bartlett, G. R. (1959) *J. Biol. Chem. 234*, 466–468.

Blasie, J. K., Schoenborn, B. P., & Zaccai, G. (1975) *Brookhaven Symp. Biol. 27*, III58–III67.

Blatt, E., & Sawyer, W. H. (1985) *Biochim. Biophys. Acta 822*, 43–62.

Blaurock, A. E. (1971) *J. Mol. Biol. 56*, 35–52.

Büldt, G., Gally, H. U., Seelig, J., & Zaccai, G. (1979) *J. Mol. Biol. 134*, 673–691.

Chattopadhyay, A., & London, E. (1987) *Biochemistry 26*, 39–45.

De Kroon, A. I. P. M., Soekarjo, M. W., De Gier, J., & De Kruijff, B. (1990) *Biochemistry 29*, 8229–8240.

East, J. M., & Lee, A. G. (1982) *Biochemistry 21*, 4144–4151.

Elliott, A. (1965) *J. Sci. Instrum. 42*, 312–316.

Everett, J., Zlotnick, A., Tennyson, J., & Holloway, P. W. (1986) *J. Biol. Chem. 261*, 6725–6729.

Franks, N. P. (1976) *J. Mol. Biol. 100*, 345–358.

Franks, N. P., & Lieb, W. R. (1979) *J. Mol. Biol. 133*, 469–500.

Franks, N. P., Arunachalam, T., & Caspi, E. (1978) *Nature (London) 276*, 530–532.

Gupta, C. M., Radhakrishnan, R., & Khorana, H. G. (1977) *Proc. Natl. Acad. Sci. U.S.A. 74*, 4315–4319.

Hargreaves, A. (1957) *Acta Crystallogr. 10*, 196–199.

Holloway, P. W., Markello, T. C., & Leto, T. L. (1982) *Biophys. J. 57*, 63–64.

Hosemann, R., & Bagchi, S. N. (1962) *Direct Analysis of Diffraction by Matter*, pp 62–64, North-Holland, Amsterdam.

Jacobs, R. E., & White, S. H. (1989) *Biochemistry 28*, 3421–3437.

Johns, H. E., & Cunningham, J. R. (1983) *The Physics of Radiology*, 4th ed., p 160, Charles C. Thomas, Springfield, IL.

Katsaras, J., & Stinson, R. H. (1990) *Biophys. J. 57*, 649–655.

King, G. I., & White, S. H. (1986) *Biophys. J. 49*, 1047–1054.

King, G. I., Jacobs, R. E., & White, S. H. (1985) *Biochemistry 24*, 4637–4645.

Kleinfeld, A. M. (1985) *Biochemistry 24*, 1874–1882.

Kleinfeld, A. M., & Lukacovic, M. F. (1985) *Biochemistry 24*, 1883–1890.

Lakowicz, J. R. (1983) *Principles of Fluorescence Spectroscopy*, Plenum Press, New York.

Lesslauer, W., Cain, J., & Blasie, J. K. (1971) *Biochim. Biophys. Acta 241*, 547–566.

Lesslauer, W., Cain, J., & Blasie, J. K. (1972) *Proc. Natl. Acad. Sci. U.S.A. 69*, 1499–1503.

Leto, T. L., Roseman, M. A., & Holloway, P. W. (1980) *Biochemistry 19*, 1911–1916.

Levine, Y. K., & Wilkins, M. H. F. (1971) *Nature New Biol. (London) 230*, 69–72.

Longmuir, K. J., Rossi, M. E., & Resele-Tiden, C. (1987) *Anal. Biochem. 167*, 213–221.

Lundblad, R. L., & Noyes, C. M., Eds. (1984) *Chemical Reagents for Protein Modification*, CRC Press, Boca Raton, FL.

Lytz, R. K., Reinert, J. C., Church, S. E., & Wickman, H. H. (1984) *Chem. Phys. Lipids 35*, 63–76.

Markello, T., Zlotnick, A., Everett, J., Tennyson, J., & Holloway, P. W. (1985) *Biochemistry 24*, 2895–2901.

Mason, R. P., Gonye, G. E., Chester, D. W., & Herbette, L. G. (1989) *Biophys. J. 55*, 769–778.

McIntosh, T. J., & Simon, S. A. (1986) *Biochemistry 25*, 4058–4066.

McIntosh, T. J., & Holloway, P. W. (1987) *Biochemistry 26*, 1783–1788.

McIntosh, T. J., Waldbillig, R. C., & Robertson, J. D. (1976) *Biochim. Biophys. Acta 448*, 15–33.

O'Brien, F. E. M. (1948) *J. Sci. Instrum. 25*, 73–76.

Pauling, L. (1960) *The Nature of the Chemical Bond*, Cornell University Press, Ithaca, NY.

Perrin, F. (1924) *C. R. Hebd. Seances Acad. Sci. 178*, 1978–1980.

Phillips, W. C., & Phillips, G. N. (1985) *J. Appl. Crystallogr. 18*, 3-7.
Press, W. H., Flannery, B. P., Teukolsky, S. A., & Vetterling, W. T. (1989) *Numerical Recipes: The Art of Scientific Computing*, pp 529-538, Cambridge University Press, Cambridge.
Runquist, E. A., & Helmkamp, G. M., Jr. (1988) *Biochim. Biophys. Acta 940*, 10-20.
Selinger, Z., & Lapidot, Y. (1966) *J. Lipid Res. 7*, 174-175.
Shannon, C. E. (1949) *Proc. Inst. Radio Eng. N.Y. 37*, 10-21.
Silvius, J. R. (1990) *Biochemistry 29*, 2930-2938.
Small, D. M. (1986) *The Physical Chemistry of Lipids*, pp 51-56, Plenum Press, New York.
Torbet, J., & Wilkins, M. H. F. (1976) *J. Theor. Biol. 62*, 447-458.
Trumbore, M., Chester, D. W., Moring, J., Rhodes, D., & Herbette, L. G. (1988) *Biophys. J. 54*, 535-543.
Warren, B. E. (1969) *X-Ray Diffraction*, pp 35-38, Addison-Wesley, Reading, MA.
White, S. H., Jacobs, R. E., & King, G. I. (1987) *Biophys. J. 52*, 663-665.
Wiener, M. C., & White, S. H. (1991a) *Biophys. J. 59*, 162-173.
Wiener, M. C., & White, S. H. (1991b) *Biophys. J. 59*, 174-185.
Wiener, M. C., King, G. I., & White, S. H. (1991) *Biophys. J.* (in press).
Worcester, D. L., & Franks, N. P. (1976) *J. Mol. Biol. 100*, 359-378.
Worthington, C. R. (1969) *Biophys. J. 9*, 222-234.
Yeager, M. D., & Feigenson, G. W. (1990) *Biochemistry 29*, 4380-4392.
Zaccai, G., Blasie, J. K., & Schoenborn, B. P. (1975) *Proc. Natl. Acad. Sci. U.S.A. 72*, 376-380.

Structure of the Rat Pancreatic Cholesterol Esterase Gene[†,‡]

Robert N. Fontaine, Christopher P. Carter, and David Y. Hui*
Department of Pathology and Laboratory Medicine, University of Cincinnati College of Medicine, Cincinnati, Ohio 45267-0529
Received November 21, 1990; Revised Manuscript Received May 9, 1991

ABSTRACT: The gene encoding the rat pancreatic cholesterol esterase has been isolated and characterized. Analysis of overlapping genomic clones showed that the cholesterol esterase gene spans approximately 8 kb, containing 11 exons interrupted by 10 introns. The exons ranged in size from 83 to 201 bp except for the last exon, which was 548 bp in length. A TAAATA sequence was present at −31 nucleotides from the transcriptional initiation site. A putative pancreas-specific enhancer sequence was found at −90 bp upstream from the CAP site. Although cholesterol esterase shares three domains of similarity with cholinesterase and acetylcholinesterase, these domains were found to be localized in distinct exons of the cholesterol esterase gene. The organization of the cholesterol esterase gene suggests its divergent evolution with other members of the serine esterase gene family.

The cholesterol esterase of the pancreas, also called carboxyl ester lipase, bile salt stimulated lipase, or nonspecific lipase, catalyzes the hydrolysis of cholesteryl esters to free cholesterol and fatty acids. The enzyme is synthesized in the acinar cells of the pancreas and is released into the intestinal lumen via the pancreatic duct (Guy & Figarella, 1981). The cholesterol esterase is one of the most abundant proteins in the pancreatic juice (Rudd & Brockman, 1984).

Current data from several laboratories (Gallo et al., 1984; Williams et al., 1989) have suggested a role of the cholesterol esterase in mediating cholesterol absorption in the gut. The cholesterol esterase has also been shown to act in concert with pancreatic lipase in lipid absorption (Lindstrom et al., 1988). In addition, the cholesterol esterase is the only enzyme in the pancreatic juice capable of hydrolyzing vitamin esters (Rudd & Brockman, 1984), suggesting its role in catalyzing the lymphatic absorption of fat-soluble vitamins from the diet.

In view of observations that the rate and efficiency of cholesterol absorption may be important determinants in regulating plasma cholesterol level and hypercholesterolemia (Kesaniemi & Miettinen, 1987), it is important to understand the regulatory mechanism(s) that may control pancreatic cholesterol esterase gene expression. Unfortunately, very little information is currently available concerning the regulation of cholesterol esterase biosynthesis under physiological conditions. The lack of progress may be related to the limited availability of information on the structure of the cholesterol esterase gene. In recent studies, progress has been made in several laboratories by cloning and sequencing of the cDNA for pancreatic cholesterol esterase from different species (Han et al., 1987; Kissel et al., 1989; Kyger et al., 1989; Hui & Kissel, 1990). In this paper, we report the isolation and characterization of the rat cholesterol esterase gene. Information obtained in this study will be useful for future studies aimed at understanding the mechanism governing the regulation of cholesterol esterase gene expression. The results of this study also suggest that the cholesterol esterase gene may have evolved differently from other members of the serine esterase gene family.

Experimental Procedures

Genomic Cloning. A rat genomic library in λ-DASH vector was obtained from Stratagene (catalog no. 247211). The genomic library was screened by the filter hybridization

[†]This research was supported by Grant DK 40917 from the National Institutes of Health.
[‡]The nucleic acid sequence in this paper has been submitted to the GenBank/EMBL database under Accession Number M69157.
*To whom correspondence should be addressed at the Department of Pathology.

0006-2960/91/0430-7008$02.50/0